Fenton-Treated Functionalized Diamond Nanoparticles as Gene Delivery System

Roberto Martín,[†] Mercedes Álvaro,[†] José Raúl Herance,[‡,*] and Hermenegildo García[†,*]

[†]Instituto de Tecnología Química CSIC-UPV and Departamento de Química, Universidad Politécnica de Valencia, Av. de los Naranjos s/n, 46022 Valencia, Spain, and
[‡]Institut d'Alta Tecnologia-PRBB, c/ Dr. Aiguader 88, 08003 Barcelona, Spain

ABSTRACT When raw diamond nanoparticles (Dnp, 7 nm average particle size) obtained from detonation are submitted to harsh Fenton-treatment, the resulting material becomes free of amorphous soot matter and the process maintains the crystallinity, reduces the particle size (4 nm average particle size), increases the surface OH population, and increases water solubility. All these changes are beneficial for subsequent Dnp covalent functionalization and for the ability of Dnp to cross cell membranes. Fenton-treated Dnps have been functionalized with thionine and the resulting sample has been observed in HeLa cell nuclei. A triethylammonium-functionalized Dnp pairs electrostatically with a plasmid having the green fluorescent protein gene and acts as gene delivery system permitting the plasmid to cross HeLa cell membrane, something that does not occur for the plasmid alone without assistance of polycationic Dnp.

KEYWORDS: diamond nanoparticles · Fenton treatment · covalent functionalization · gene delivery · GFP expression.

Inclusion of nanoparticles inside living cells is a topic of much interest since it can be used as a drug delivery system and it can be applied for the treatment of various diseases.[1] One of the requirements of the nanoparticles to be used as drug carriers and in diagnosis is the absence of remarkable cytotoxicity.[2−4] In this context it has been recently reported that diamond nanoparticles (Dnps) exhibiting fluorescence can cross the cell membrane and become localized in the cytoplasm.[5] Using laser ablation a high concentration of 1.7×10^{18} of light emitting nitrogen-vacancy defects leading to phonon absorption at 470 nm and light emission at 530 nm has been recently reported.[6,7] Because of the structure and composition of Dnps, they are remarkably biocompatible causing minor cell mortality.[2−4] When highly fluorescent, these Dnps can be used as biomarkers since they can cross the cell membrane.[6−8] Recently Dnps have also been used as drug carriers and for the covalent and electrostatic binding of active biomolecules,[9−13] opening new avenues for expanding the applications of these materials in biomedicine.[14] Besides the low toxicity and the ability to cross the cell membrane one of the main advantages of Dnps is that they can be prepared in large quantities by detonation of explosives and have become commercially available.[15−17] However the as-synthesized raw materials, in addition to crystalline Dnp, contain amorphous carbon generally denoted as "soot matter". This soot matter covers the diamond nanoparticles causing Dnp agglomeration and making their functionalization as well as their dispersion in a liquid phase difficult.[15] Actually the preparation of suitably functionalized Dnps with organic moieties to implement new properties on the otherwise inert Dnps is a topic of much interest per se.[1,18] Recently we have shown that aggressive Fenton treatment can serve to remove in a considerable extent undesirable soot matter while at the same time introducing a large density of surface hydroxyl groups that can be subsequently used as sites for the covalent anchoring of alkyl chains or aromatic rings.[19]

Considering the above precedents on the biocompatibility of raw Dnp, it occurred to us that we should be able to improve the inherent ability of raw Dnps to cross cell membranes by submitting the sample to a prior Fenton treatment and subsequent functionalization.

In this manuscript we show that Fenton-treated and subsequently functionalized Dnps cross the cell membrane bearing the subunit bonded to them and can reach the nucleus, something that in earlier reports was found not to occur for raw Dnp not submitted to Fenton treatment.[20] Related precedents reporting that Dnp can enter the cell samples containing soot matter have been studied. The main originality of

*Address correspondence to hgarcia@qim.upv.es, Raul.Herance@crccorp.es.

Received for review June 30, 2009 and accepted December 23, 2009.

Published online January 4, 2010.
10.1021/nn901616c

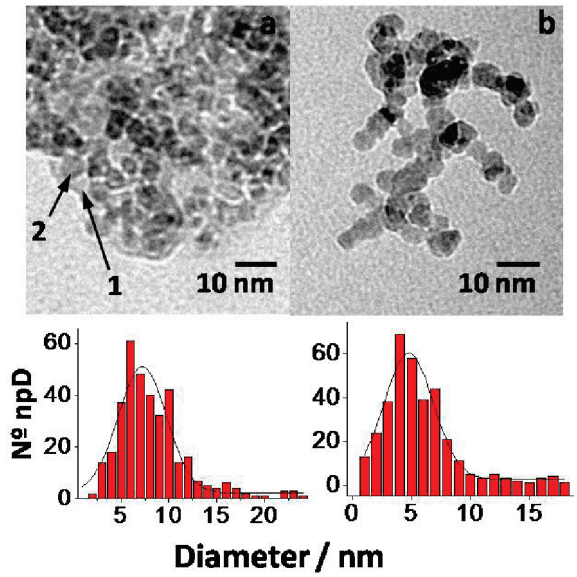

Figure 1. Selected TEM images and particle size distribution of pristine Dnp (a) and HO−Dnp (b). Soot matter (1) and Dnp (2) are marked in image a for clarity.

our work is to show that Fenton-treated Dnp with significantly different morphological and chemical properties with respect to commercial samples exhibit a much enhanced performance for functionalization and for entering into the cell than the previously used materials. The ease and high density of this surface functionalization process endows Dnps with a significant advantage over other nanomaterials for specific or nonspecific binding with organic moieties and biomolecules such as nucleic acids. Therein by attaching a fluorescent molecule we have obtained images that indicate that these nanoparticles can reach the cell nuclei. We have taken advantage of this ability of Fenton-treated Dnp to enter into cells and have used them as gene carriers to introduce a plasmid that has an enhanced activity to express the green fluorescent protein (EGFP) in human cervical cancer (HeLa) cells. In all cases a good biocompatibility was observed.

RESULTS AND DISCUSSION

Fenton Treatment. A commercial sample of Dnp obtained by detonation was submitted to the Fenton reaction using H_2O_2 and $FeSO_4$ under strong acidic conditions. Transmission electron microscopy (TEM) images of the sample before (Dnp) and after Fenton treatment (HO−Dnp) show that this reaction causes an almost complete disappearance of the amorphous soot matter (Figure 1). In addition we also noticed a decrease in the average particle size of the diamond nanoparticles from 7.20 nm for Dnp to 4.77 nm for HO−Dnp.

We interpret this particle size reduction as a consequence of the surface erosion by the chemical reaction that is known to produce the decomposition and partial mineralization to CO_2 of organic compounds.[11,21,22] In agreement with this rationalization comparison of the

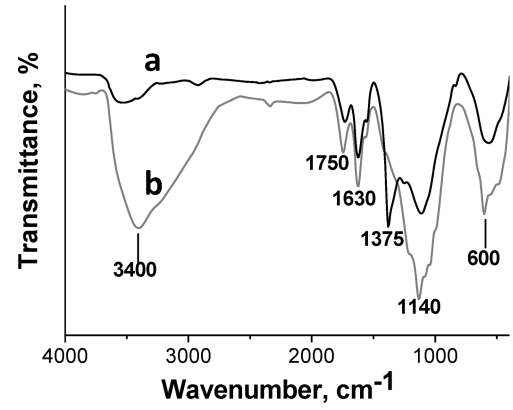

Figure 2. FT-IR spectra of pristine Dnp (a) and Fenton treated HO−Dnp sample (b).

IR spectra of samples before (Dnp) and after the Fenton treatment (HO−Dnp) shows an increase in the population of hydroxyl groups. Figure 2 shows the corresponding IR spectra of raw and Fenton-treated Dnp. Since the same weight of samples was used for recording all FT-IR spectra, this technique allows quantitative estimation of the increase on the population of OH groups. Thus, the area of the band centered at 3400 cm^{-1} is directly related to the increase in the population of the OH groups. As can be seen there, Fenton treatment produces a 12-fold increase in the density of the OH groups while at the same time an increase in the band at 1140 cm^{-1} corresponding to C−O single bond is observed.

The increase in the population of surface hydroxyls is the reason why the sample after Fenton treatment is denoted HO−Dnp. A consequence of this increase of the density of hydroxyl groups in the diamond nanoparticles sample is the increase in its water solubility after the Fenton treatment. This solubility (4 mg mL^{-1}) is a reflection of the high hydrophilicity of the sample produced by the presence of surface −OH groups. Commercial raw Dnp samples do not form persistent colloidal suspensions in water, and all the suspended material settles down upon standing the suspension for a few minutes. In contrast after Fenton treatment, the particle size reduction, disappearance of the soot matter, and the increase of the surface OH groups favor the formation of colloids in water. This has allowed us the experimental determination of average particle size, size distribution, and z-potential point of the colloids. At the same time powder XRD shows that the diamond nanoparticles after the treatment still maintain the diffraction pattern characteristic of crystalline diamond.

Therefore the available characterization data indicates that the Fenton treatment used removes undesirable soot matter, produces disaggregation of Dnp decreasing the average size, and increases the density of the surface hydroxyl groups and solubility. All these

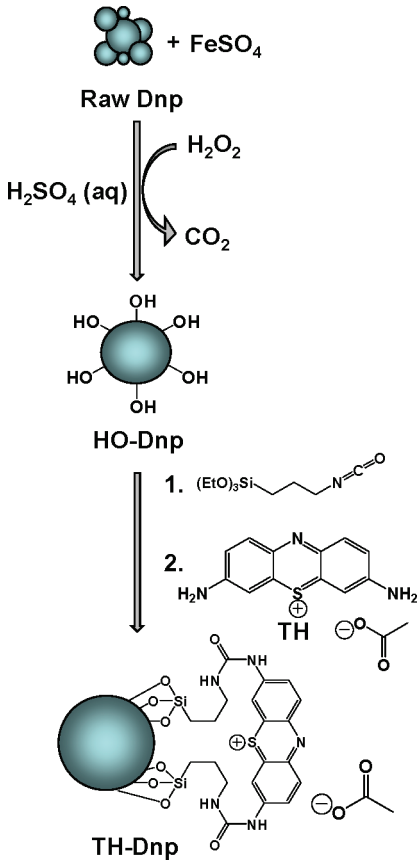

Scheme 1. Synthetic route followed to obtain TH−Dnp.

features should be in principle favorable for the inclusion of this material into living cells.

Covalent Functionalization. Using Fenton-treated diamond nanoparticles and in order to demonstrate their ability to be incorporated into the cells, we proceeded to the covalent functionalization of these HO−Dnp nanoparticles with a highly fluorescent organic dye that could be detectable inside living cells by fluorescence microscopy in the case where the HO−Dnp enters the cell membrane. For our study we selected thionine (TH) and effect the covalent attachment of this fluorescent molecule to HO−Dnp in two steps using a propyl carbamate tether as linker. Scheme 1 depicts the synthetic route followed to obtain the target TH-functionalized diamond nanoparticles (TH−Dnp). In the first step isocyanate-terminated diamond nanoparticles are obtained and subsequently submitted to nucleophilic addition with thionine in the second reaction.

The resulting TH−Dnp sample was characterized by combustion chemical analysis and spectroscopic techniques. The TH content (12.95%) in the sample was quantified on the basis of the sulfur content since this element is specific of thionine. Also the increase of the percentage of nitrogen from the intermediate isocyanate nanoparticles to TH−Dnp is in agreement with the sulfur content confirming the TH loading in the TH−Dnp sample. The presence of TH and its structural integrity in the TH−Dnp sample can be assessed by optical and vibrational spectroscopy. Considering the solubility of TH−Dnp in water, the UV−vis spectrum of TH−Dnp was recorded in transmission mode from the aqueous solution of TH−Dnp nanoparticles. The spectrum is shown in Figure 3 where a comparison with analogous UV−vis spectra of Fenton-treated HO−Dnp and TH is also shown. As can be seen in Figure 3 the observation of a band at 630 nm showing a shoulder in the blue side of the peak indicates the presence of the organic dye in TH−Dnp. We also notice a red shift in λ_{max} for the TH chromophore from 598 to 625 nm when it becomes attached to the nanoparticles and an increase in the bandwidth. The bandwidth is commonly associated with the formation of aggregates, a phenomenon that is generally observed in tricyclic basic dyes as TH.[23,24] Since the TH units should be anchored on the surface of HO−Dnp in close proximity with immobilized neighbors the formation of TH aggregates should be favored with respect to solution due to a concentration effect.

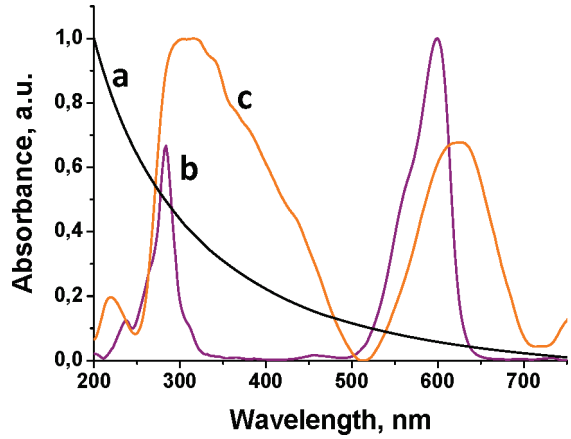

Figure 3. Absorption spectra of deareated aqueous solutions of HO−Dnp (a), thionine acetate (b), and TH−Dnp (c).

Also FT-IR spectroscopy reveals the presence of TH groups in TH−Dnp based on the coincidence of the peaks in the 1620−1400 cm^{-1} region corresponding to the aromatic vibration of TH rings. The presence of TH and the covalent attachment is also supported by the observation of a strong band at 1742 cm^{-1} corresponding to the carbamate group.

In addition, a deeper comparison of the FT-IR spectra for −OH diamond nanoparticles and TH−Dnp shows a remarkable decrease in the intensity of the −OH groups responsible for the 3400 cm^{-1}. This fact is compatible with the functionalization of −OH groups in HO−Dnp when TH−Dnp is formed as indicated in Scheme 1. TEM image in Figure 4 shows no changes in the morphology of HO−Dnp upon the covalent grafting of TH moieties, the average particle size of TH−Dnp being statistically coincident with that measured for HO−Dnp. The solubility of TH−Dnp in water was higher than of OH−Dnp (>4 mg/mL).

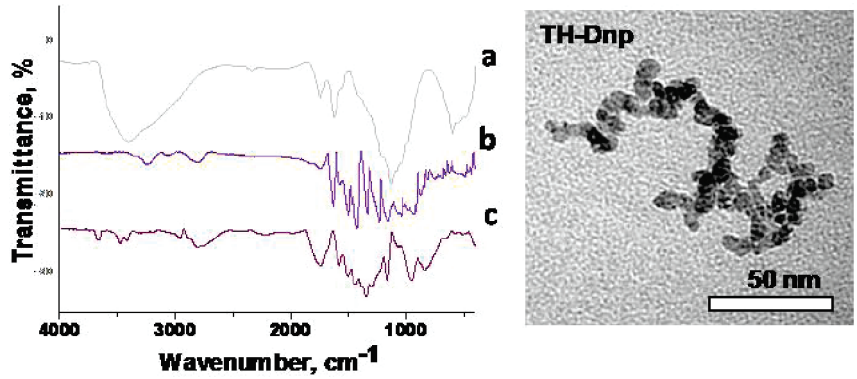

Figure 4. (Left) FT-IR spectra of HO−Dnp (a), thionine acetate (b), and TH−Dnp (c). (Right) Representative TEM image of TH−Dnp sample from which an average particle size of 5.8 nm has been determined.

Laser scattering of TH−Dnp colloidal solutions in water have shown that the average particle size present in the aqueous phase is 140 nm. This average size indicates that because of the tendency of nanometric particles to agglomerate, the colloids present in water are in reality aggregates of TH−Dnp. In any case this colloid average particle size is still remarkably small in the submicrometric size.

For our purposes of detecting the incorporation of TH−Dnp inside the cells, one important property is the ability of thionine to emit red fluorescence upon excitation at 598 nm. Figure 5 compares the fluorescence and excitation spectra of TH and TH−Dnp. Although some diminution in the emission quantum yield of TH can occur in TH−Dnp as consequence of aggregation of TH units on the diamond surface,[23−25] the emission spectrum shown in Figure 5 clearly indicates that the TH−Dnp are still emissive nanoparticles upon photo excitation at long wavelengths. Unfortunately due to light scattering of TH−Dnp colloidal suspensions accurate numbers of fluorescence quantum yield could not be obtained.

One process analogous to the one used for the preparation of TH−Dnp based on surface silylation was used for the synthesis of a sample of diamond nanoparticles containing quaternary tetraethyl ammonium groups (TEA−Dnp). The synthetic route followed for TEA−Dnp is also indicated in Scheme 2. The target TEA−Dnp was again obtained in two steps starting from HO−Dnp by reacting them with 3-iodopropyl triethoxysilane and carrying out the nucleophilic substitution of iodo by triethylamine.

The rationale behind the preparation of this quaternary ammonium salt was to obtain a cationic polyelectrolyte based on diamond nanoparticles that eventually could be used for delivery of a plasmid inside the cell due to noncharged plasmid−ND complex. The percentage of quaternary ammonium groups in TEA−Dnp (15 wt %) was determined by combustion chemical analysis based on the percentage of nitrogen. Figure 6 shows a comparison of the FT-IR spectra of TEA−Dnp and the iodopropylsilyl derivative of HO−Dnp. Also Figure 6 shows TEM images of TEA−Dnp showing no changes in the morphology of the Fenton-treated Dnp upon functionalization with TEA units. TEM confirms the lack of significant changes in the particle size of Dnp upon introduction of the TEA groups. In addition no noticeable changes in the solubility (>4 mg/mL) inherent to HO−Dnp by the presence of TEA were observed. Laser scattering of colloidal TEA−Dnp solutions in water shows that the average diameter of the colloidal particles in water is 295 nm. Again as in the case of TH−Dnp, for TEA−Dnp aggregation of primary

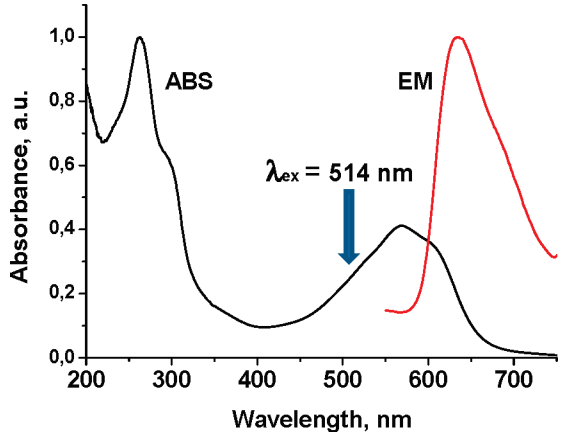

Figure 5. Emission (EM, λ_{exc} = 514 nm) and absorption (ABS) spectra of TH−Dnp recorded in solid state.

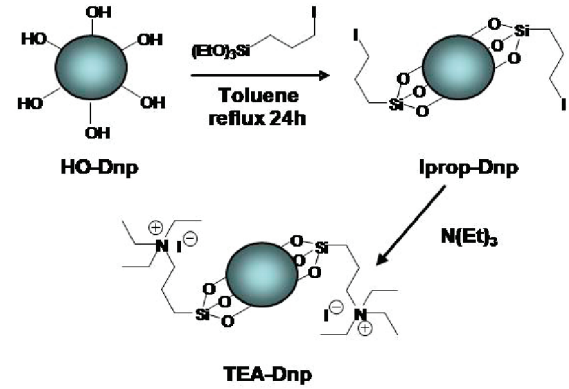

Scheme 2. Synthetic route followed to prepare TEA−Dnp.

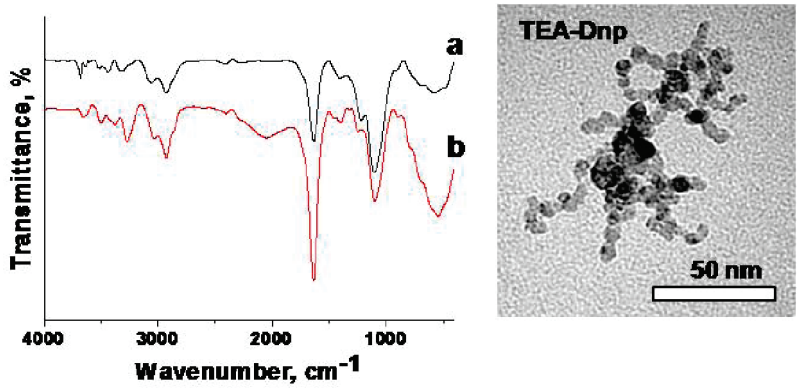

Figure 6. (Left) FT-IR spectra of Iprop−Dnp (a) and TEA−Dnp (b). (Right) TEM image of TEA−Dnp sample showing the same morphology and average particle size as parent HO−Dnp.

particles observed by TEM occurs when this material is suspended in water.

Cell Incubation Tests. As indicated in the introduction the purpose of our work was to show the improved performance and suitability of Fenton-treated diamond nanoparticles in biological studies. Thus we proceeded to introduce TH−Dnp in the culture medium where HeLa cells were grown. After 24 h incubation, as shown in Figure 7, fluorescence microscopy images indicate that the characteristic red fluorescence due to TH is present inside the nuclei. Also some TH−Dnp particles have been observed in cytoplasm. We monitored the cytotoxicity effects of TH−Dnp on HeLa cells by quantitative flow cytometry analysis. We have determined that 97% of HeLa cells survived after incubation with TH−Dnp, a value that is very similar for the HeLa cells incubated in the absence of TH−Dnp. These results show that TH−Dnp exhibits very good biocompatibility.

We also noticed, by analysis of the nuclear morphology at 72 h, nuclei appeared round, clear-edged, and uniformly stained indicating these cells were not apoptotic.

To take better images of the location of TH−Dnp into the nuclei, we used DAPI that is a selective staining dye for the nuclei. The use of DAPI reveals that TH−Dnp is inside the nucleii forming aggregates appearing as red spots in the regions complementary to the blue emission of DAPI. Thus, it appears that small sized diamonds are able to enter the nucleus. Figure 7 shows a selected set of confocal fluorescence images and fluorescence mode showing the location of modified TH−Dnp diamond nanoparticles with respect to DAPI. To put into context the images shown in Figure 7 it should be mentioned that related precedents working with raw diamond nanoparticles have found that this material does not enter the cell nucleus and it is localized in the cytosol.[3,4,20] Therefore the results shown in Figure 7 are unique and without precedent. We propose that they derive from the change in morphology, size, and increased compatibility by the surface OH groups of the diamond nanoparticles caused by the Fenton treatment.

Further confirmation of the location of TH−Dnp into the nucleus was obtained by z-stack scanning of the confocal microscopy images recorded in fluorescence mode. By changing the vertical distance of the image it was observed that the red fluorescence characteristic of TH−Dnp is observed in the image recorded in the middle but not when the confocal plane was at the top or bottom of the cell. Figure 8 show a set of three merged (blue and red fluorescence) confocal images recorded at different vertical confocal distance.

Another aspect of interest is that in previous works laser ablation has been used to promote fluorescence of Dnp.[3−5] Another advantage of Fenton treatment

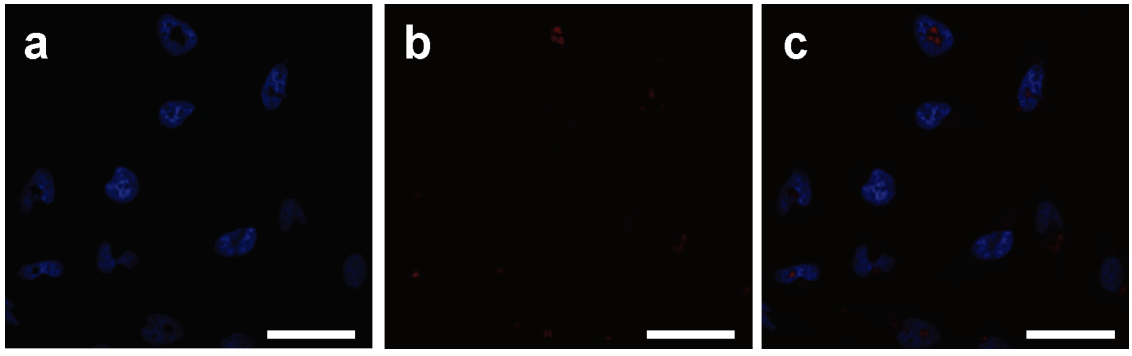

Figure 7. Confocal microscopy images taken at fluorescence mode (λ_{ex} = 405 nm) (a), fluorescence mode (λ_{ex} = 514 nm) (b), and merged images (c), showing the DAPI-stained nuclei (a) and the location of modified diamond nanoparticles containing thionine (b and c) (Scale bar is in all cases 50 μm).

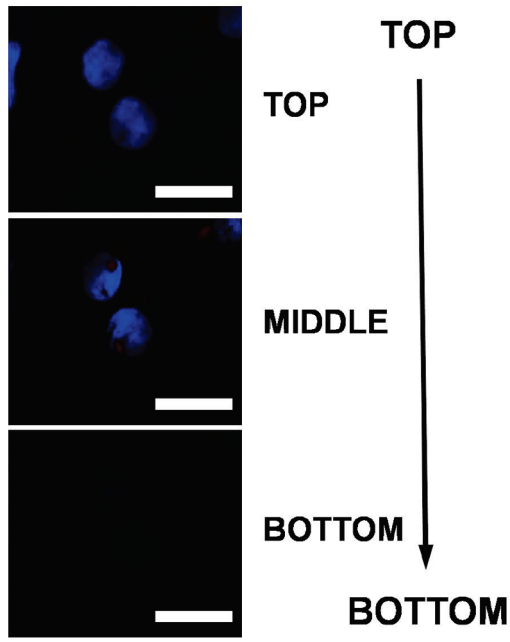

Figure 8. *Z*-axis scanning images of TH−Dnp in a HeLa cells by laser scanning confocal microscope obtained merging the blue (DAPI) and red (TH−Dnp) fluorescence. The red spots indicating the location of TH−Dnp were obtained exciting at 514 nm and the emission was collected in the range of 670−770 nm. The blue spots correspond to the DAPI stained nuclei obtained exciting at 405 nm and the emission collected in the range of 415−485 nm. Scale bars are 25 μm in all cases.

followed by covalent attachment of a fluorophore with respect the fluorescence reported for diamond laser ablated nanoparticles is the size reduction and removal of the soot matter. This leads to smaller Dnp nanoparticles after Fenton treatment compared to laser ablation.[19] Since the equipment necessary for laser ablation is not routine, this procedure to introduce fluorescent diamond nanoparticles requires a specific setup and instrumentation.[5] In contrast Fenton treatment creates enough −OH density to allow sufficiently high loading of a fluorescent probe that can be used to determine the location of the diamond nanoparticles in the cell. Also different dyes can be attached leading to emission in different wavelengths. Since Fenton reaction does not require special equipment, our procedure can be versatile for amenable production of fluorescent diamond nanoparticles.

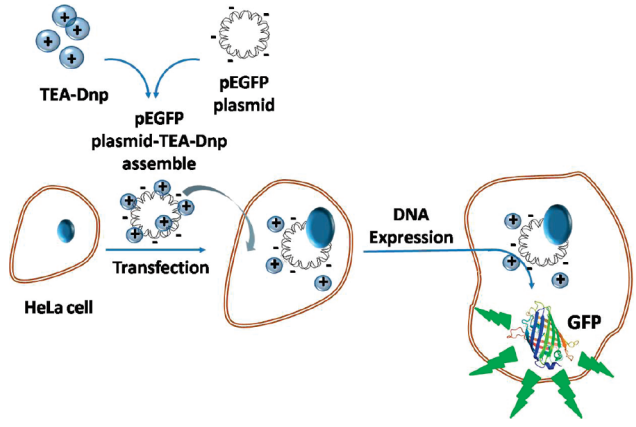

Scheme 3. Diagram of the transfection experiment using pEGFP plasmid and TEA−Dnp as gene carrier for cyclic pEGFP plasmid.

Encouraged by the previous results showing that small and fairly disaggregated diamond nanoparticles can reach the cell nuclei, we have used TEA−Dnp as a polyelectrolyte that interacts strongly by ion pairing with a plasmid. In the present study we have used a pEGFP plasmid that has been demonstrated not to enter into the cell through the membrane on its own[20] and, on the other hand, it contains a sequence for the enhanced expression of the green fluorescent protein (GFP) when is effectively transcribed by the cell machinery. Scheme 3 depicts the experiment using pEGFP plasmid and TEA−Dnp as carrier and shows the different steps leading to the efficient production of EGFP and its detection by fluorescence microscopy.

Therefore, the experiment consists in assuming that Coulombic interaction and ion pairing between positive ammonium-modified TEA−Dnp nanodiamonds and the negatively charged pEGFP plasmid will form a strong assembly that could cross the cell membrane. In other words, while plasmid alone does not enter the cell it is expected that by coupling with modified TEA−Dnp nanodiamonds, the latter would act as carrier delivering the plasmid inside the cell. If this were the case, then the plasmid by making use of the intracellular machinery could be efficiently translated into EGFP protein whose formation will be detected by fluorescence microscopy.

When HeLa cells were incubated in the presence of the plasmid with the EGFP coding sequence in the absence or presence of TEA-modified Dnp, green fluorescence was observed only in the case where the plasmid and TEA−Dnp were present. The lack of observation of green fluorescence in the absence of TEA−Dnp is consistent with the previous known inefficiency of the pEGFP plasmid to cross the cell membrane.[20] In contrast, observation of green fluorescence when both the plasmid and TEA−Dnp were present indicates the expression of EGFP and, therefore, this is a safe confirmation that the plasmid has managed to enter the cell as a result of pairing with modified TEA−Dnp diamond nanoparticles. Figure 9 shows selected phase contrast and fluorescence images to illustrate the results obtained in the experiments with the plasmid depending on the presence or absence of TEA−Dnp.

To provide alternative evidence supporting GFP expression in the cell when they are incubated in the presence of the plasmid and TEA−Dnp, we performed a Western blot analysis using as control the same cells in the presence of the plasmid incubated without TEA−Dnp. The results of the Western blot are shown in Figure 10. In this electrophoretic assay, observation of similar amounts of tubulin ensures that a similar loading of proteic material has been charged in the control

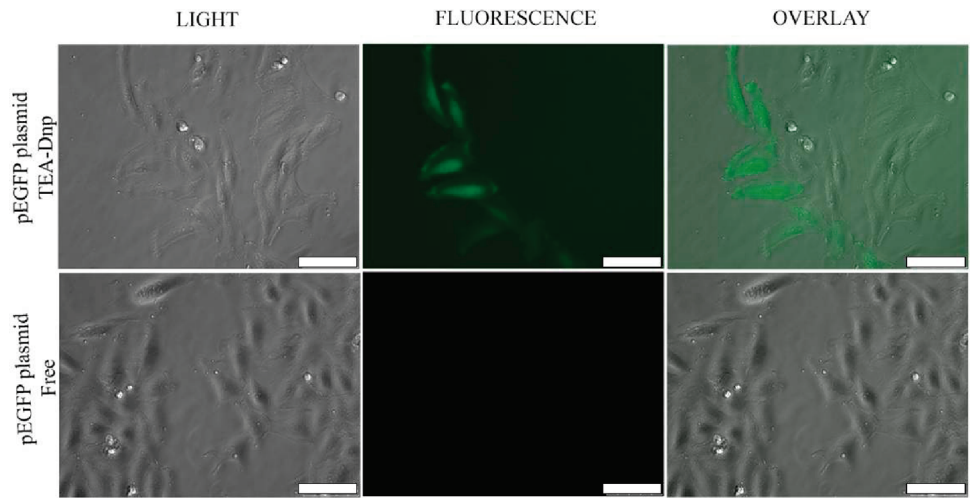

Figure 9. (Top) Images of HeLa cells with pEGFP plasmid-TEA−Dnp assembly after 48 h showing EGFP expression by light microscope, fluorescence microscope (λ_{ex} = 488 nm), merged image (combined light and fluorescence images). (Bottom) pEGFP plasmid in the absence of TEA−Dnp by light microscope, fluorescence, and merged image (combined light and fluorescence images). Scale bars are 75 μm.

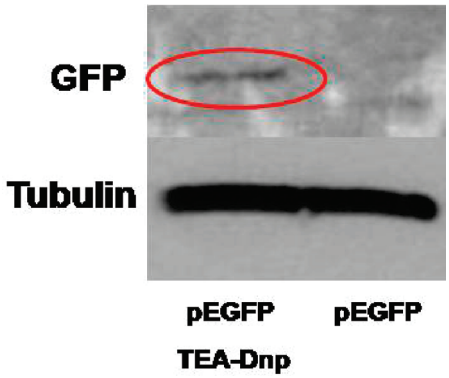

Figure 10. Western blot expression analysis of GFP protein in HeLa cells incubated with pEGFP-TEA−Dnp and control cells incubated with pEGFP free. The GFP expression band can only be detected in cells incubated with pEGFP-TEA−Dnp; 60 μg of protein were used. Tubulin was used as a loading control.

and in the culture where the plasmid and TEA−Dnp were present. As it can be seen in Figure 10 the band corresponding to the GFP is observed when the cell is incubated in the presence of TEA−Dnp but not in the control in where TEA−Dnp was absent. The result of the Western Blot agrees with the results of the fluorescence microscopy since the result of the GFP expression of the plasmid is the observation of fluorescence.

To determine cell viability as a function of TEA−Dnp concentration, quantitative flow cytometry analysis of viability after treatment with pEGFP-TEA−Dnp or pEGFP free for 3 h was measured. The results are shown in Figure 11. As it can be seen there, both analyses of viability in the presence and absence of TEA−Dnp are significantly coincident showing that the presence of TEA−Dnp does not influence cell viability unless the concentration is 1 order of magnitude larger than the concentration employed for gene delivery.

There are in the literature different transfection vectors that can be used to facilitate the cellular inclusion of DNA inside cells including viruses, charged lipids, and cationic molecules;[26−31] however, with respect to this transfection vectors diamond nanoparticles combine a series of properties that could make them be the preferred system under certain circumstances. Thus, due to the low mortality of these nanoparticles, HO−Dnp can

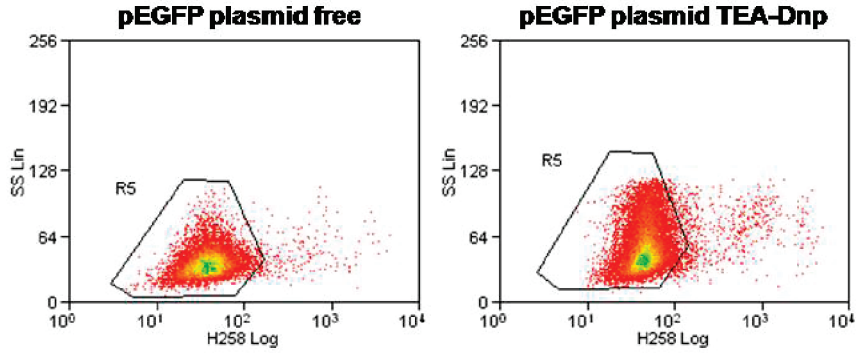

Figure 11. Quantitative flow cytometry analysis of viable cells after treatment with pEGFP free or with pEGFP-TEA−Dnp assemble. The cells were stained after 48 h with propidium iodide and analyzed by flow cytometry. Propidium iodide readily enters and stains nonviable cells, but cannot cross the membrane of viable cells. The R5 quadrant represents live cells. A total of 15000 cells were measured for the viability analysis.

be functionalized through a large variety of organic transformations, are chemically inert, and also permits a high loading derived from the high population of surface OH groups.

CONCLUSION

In the present work we have shown that Fenton reaction is an advantageous treatment to activate diamond nanoparticles since it produces the disappearance of soot matter, the disaggregation of Dnp, the reduction of the average particle size, and the increase in the population of surface hydroxyl groups as well as water solubility.

By covalent functionalization of this Fenton-treated Dnp with a fluorescent dye we have shown that these nanoparticles enter HeLa cells, some reaching the cell nuclei. Since previous studies using Dnp have not observed the entrance of Dnp into the cell nuclei it is very likely that our finding derives from the special features introduced as a consequence of the Fenton treatment. In addition this chemical treatment produces a material with high biocompatibility determined after 72 h incubation.

In addition the ability of Dnps to cross the cell membrane has been exploited to assist the intracellular delivery of a plasmid that later expresses its genetic charge forming the GFP. This demonstrates the use of Dnp as carriers preserving the biological activity of the accompanying cargo.

With respect to other transfection vectors, Fenton-treated Dnp are noncytotoxic, can be functionalized through many different reactions, and may allow a high loading of bioactive moiety.

METHODS

Materials and Instrumentation. All the solids were analyzed by combustion chemical analysis (C, H, N, and S) performed in a FISONS CHNOS analyzer. UV−vis spectra were recorded in transmission mode on a Shimadzu UV−vis spectrophotometer. The samples were placed in quartz cuvettes of 1 cm path length. FT-IR spectra were recorded on a Nicolet 710 FT-IR spectrophotometer using KBr disks or self-supported wafers (10 mg) compressed to 2 Ton cm^{-2} for 2 min. The size of the nanoparticles was determined by transmission electron microscopy (TEM) using a Philips CM300 FEG system with an operating voltage of 100 kV. TEM samples were prepared by placing microdrops of diamond nanoparticles solution directly onto a copper grid coated with carbon film (200 mesh). Unless otherwise indicated, solvents and reagents were purchased from Aldrich and used as received. Powder XRD was recorded using a Philips X'Pert diffractometer using the Cu Kα radiation at a scan rate of 2° min^{-1}.

Fenton Treatment. Raw Dnp (1 g) commercially available from Aldrich (Diamond nanopowder, 95+%; ref, 636444) was suspended in distilled water (50 mL) in a 500 mL open flask and mixed directly with $FeSO_4 \cdot 7H_2O$ (20 g) as source of Fe^{2+}. After complete dissolution of the ferrous salt, concentrated sulfuric acid (30 mL) was added to the slurry and the corresponding volume of H_2O_2 (30 v/v %) (20 mL) was slowly dropped while observing evolution of CO_2. (Caution: The Fenton reaction is highly exothermic and occurs with evolution of heat and gases. The process has to be done in a well ventilated fume hood wearing the appropriate personal safety items). This slurry was sonicated on an ice-refrigerated ultrasound bath and held at 1−5 °C for 5 h. Within the first 30 min, the solution turned green/yellow colored, indicative of iron oxidation After 1 h, additional amounts of H_2SO_4 and H_2O_2 were added while the suspension became yellowish. This second cycle consisting in the addition of reagents and sonication can be repeated, allowing the final cycle to occur for longer times to ensure the complete decomposition of H_2O_2.

After the Fenton treatment, the suspensions were diluted with distilled water and allowed to reach room temperature. The excess of acid was removed by performing five consecutive centrifugation−redispersion cycles with Mili-Q water. The diamond nanoparticles settled at the bottom of the centrifuge tube under these conditions. The pH value of the supernatant at the fifth centrifugation−redispersion cycle was neutral. Finally, the Fenton-treated Dnps were submitted to overnight freeze-drying to obtain a brownish dustlike material. Up to 4 mg of HO−Dnp could be dissolved in 1 mL of Milli-Q water.

Culture of HeLa Cells. HeLa cells were cultured in Dulbelcco's modified eagle medium (DMEM from Gibco) supplemented with 10% fetal bovine serum (FBS from Gibco), 100 U/mL penicillin, 100 μg/mL streptomycin (Gibco), and 2 mM L-glutamine (Gibco). The cells were cultured at 37 °C in 5% CO_2 atmosphere.

Incubation of Living Cells with TH−Dnp Solutions. The cells were seeded at a concentration of 17000 cells/well in 12-well plates (Corning, NY 14831) containing 1 mL of medium and 15 mm of diameter plastic coverslips treated for cell culture (Thermanox Plastic Coverslips, NUNC) in the bottom. The cells were left at 37 °C in 5% CO_2 atmosphere overnight in order to attach.

The next day, the medium was replaced for a suspension of 20 μg/mL of TH−Dnp in HeLa medium and incubated for 24 h. The diamond nanoparticles parent solution was prepared by suspending 1 mg of TH−Dnp in DMSO (Sigma-Aldrich) to a final concentration of 750 μg mL^{-1}. The use of DMSO facilitates TH−Dnp dissolution and a more homogeneous dispersion in the culture media. For control cells, a suspension of 20 μg/mL of thionine in HeLa medium was incubated for 24 h.

After 24 h incubation with TH−Dnp, or thionine acetate for control cells, at 37 °C in 5% CO_2 atmosphere, the media was removed, the cells were washed with sterile phosphate buffered saline solution (PBS) pH 7.4 (Invitrogen) four times and fixed with 4% paraformaldehyde for 20 min at room temperature. After fixation, the cells were washed 3 times with PBS and stained with 4′,6-dimidino-2-phenylindole (DAPI) (Invitrogen, 21490, 1:10000) for 10 min at room temperature. After this time, the coverslips were set on top of microscope slides covered with mounting medium and a 24 × 40 mm coverslip (Knittel Glass) on top. Fluorescence images were taken using Leica SP5 confocal microscope. For the fluorescence imaging of DAPI, the sample was excited with a 405 nm UV laser and fluorescent emission was obtained between 415−485 nm. For the fluorescence imaging of TH−Dnp particles, the sample was excited with a wavelength of 514 nm and fluorescent emission was obtained between 714−800 nm.

For the fluorescence imaging of Thionine alone, the sample was excited also at wavelength of 514 nm and fluorescent emission was monitored between 670−770 nm.

Z-scanning images were recorded by merging the blue (DAPI) and red (TH−Dnp) emissions using the confocal microscope with a vertical resolution of about 0.3 μm.

Viability Analysis. HeLa cells were seeded the day before at about 40000 cells/well in 24-well plates. A 20 μg/mL solution of TH−Dnp in DMSO was mixed. In the case of TEA−Dnp the nanoparticles were combined with 250 ng of plasmid pEGFP in a ratio of 10:1, in ng of TEA−Dnp:pEGFP. The solution was vortexed for 10 s and then was incubated for 90 min at room temperature to allow pEGFP-TEA−Dnp complex formation. After this incubation, 400 μL of pEGFP-TEA−Dnp or TH−Dnp solution was added to each well of 24-well plates containing HeLa cells. pEGFP-TEA−Dnp or TH−Dnp was left to incubate with the cells for 3 h. After the incubation, the medium solution was removed and replaced with fresh medium. Control solutions were carried out with the same preparation procedure but without TEA−Dnp or TH−Dnp.

After 48 h, cells were washed with warm PBS and trypsinizated with 0.25% trypsin−EDTA (Invitrogen) for 5 min, after this time, trypsin was inactivated with HeLa medium. Cells were collected by centrifugation (2000 rpm, 3 min) and resuspended in 500 μL of PBS. A 100 μL portion of propidium iodide (P4170, Sigma-Aldrich) solution (0.5 mg/mL in PBS with 0.1% sodium azide, pH approximately 7.4) was added to 500 μL of cell suspension and left to incubate for 5 min. Propidium iodide binds to double-stranded DNA. Propidium iodide absorbs in blue-green (493 nm) and fluorescence can be detected in red (630 nm). Finally cells were analyzed on a MoFlo cell sorter (DakoCytomation) with Summit software. A total of 15000 events were collected for the cell viability analysis.

Nanoparticle Transfection Using pEGFP Plasmid-TEA−Dnp. HeLa cells were seeded the day before at about 40000 cells/well in 24-well plates. One mg of cationic TEA−Dnps nanodiamonds was dispersed in DMSO (Sigma-Aldrich) to a 20 μg/mL solution and sonicated for 10 min. Different aliquots of the parent solution were taken and added to OptiMEM (Gibco) medium until a final volume of 200 μL. A 250 ng portion of plasmid pEGFP containing an EGFP coding sequence under a CMV promoter (Clontech) was dissolved in OptiMEM medium to a final volume of 200 μL.

A ratio 10:1, in ng of TEA−Dnp:pEGFP was prepared mixing 200 μL of the solutions prepared previously in a 1.5 mL eppendorf tube. The solution was vortexed for 10 s and then was incubated for 90 min at room temperature to allow pEGFP-TEA−Dnp complex formation. After this incubation, the 400 μL of pEGFP-TEA−Dnp solution was added to each well of 24-well plates containing HeLa cells. pEGFP-TEA−Dnp was left to incubate with the cells for 3 h. After the incubation, the pEGFP-TEA−Dnp medium solution was removed and replaced with 400 μL of fresh medium. Images were taken after 48 h using Leica DMI 4000B microscope.

Different control solutions with the same preparation procedure were carried out without TEA−Dnp, but pEGFP incorporation in HeLa cells in the absence of these was not observed.

Western Blot Analysis. Cells were washed twice with cold PBS then harvested by scraping cells in ice-cold lysis buffer consisting of Tris-HCl pH 7.4 (Roche), 250 mM NaCl, 1% Triton X100, 1 mM EDTA, 1 mM EGTA, 0.2 mM PMSF (all Sigma-Aldrich Química), 1X protease inhibitor cocktail (Roche), and 1X phosphatase inhibitor cocktail (Sigma-Aldrich Química). Lysates were passaged through a 1 mL syringe (Rubilabor) and a 25G needle (Terumo) and left for 30 min on ice. Lysates were clarified by centrifugation at 10000 rpm for 10 min at 4 °C, and protein concentrations were determined by Bradford assay (Bio-Rad Laboratories GmbH). A 60 μg portion of protein was mixed with 4× of a commercial loading buffer (Invitrogen) containing 20% 2-mercaptoethanol (Sigma-Aldrich Química), boiled at 100 °C for 5 min and resolved on 8−12% SDS polyacrilamide electrophoresis gels. After electrophoresis, proteins were transferred to a nitrocellulose membrane using a submerged transfer apparatus (BioRad), filled with 25 mM Tris Base (Roche), 200 mM glycine (Sigma-Aldrich Química), and 20% methanol (Merck). Membranes were blocked in PBS containing 0.1% Tween-20 (PBST) (Sigma-Aldrich Química) and 5% milk powder (Sigma-Aldrich Química) for 1 h at room temperature. Membranes were incubated with primary antibody in PBST supplemented with 2% milk powder overnight at 4 °C. Primary antibodies were raised against GFP monoclonal antibody (clones 7.1 and 13.1, Roche) used as a 1:400 dilution and against alfa-tubulin (T6074, Sigma-Aldrich) used as a 1:8000. Membranes were washed four times at room temperature for 5 min in PBST, then incubated for 1 h at room temperature with horseradish peroxidase (HRP)-conjugated secondary antimouse antibody (Amersham Biosciences) as a 1:4000 dilution in PBST 2% milk powder. HRP activity was detected using ECL Plus detection kit (Pierce) following manufacturer's instructions on Amersham ECL Hyperfilm (GE Healthcare, Limited).

Acknowledgment. Financial support by the Spanish ministry of Science (CTQ2006-06785 and CTQ2007-67805-AR07) is gratefully acknowledged. R.M. also thanks Spanish Ministry of Education for a postgraduate scholarship.

REFERENCES AND NOTES

1. Krueger, A. New Carbon Materials: Biological Applications of Functionalized Nanodiamond Materials. *Chem.—Eur. J.* **2008**, *14*, 1382–1390.
2. Schrand, A. M.; Huang, H; Carlson, C; Schlager, J. J.; Osawa, E.; Hussain, S. M.; Dai, L. Are Diamond Nanoparticles Cytotoxic? *J. Phys. Chem. B* **2007**, *111*, 2–7.
3. Shu-Jung, Yu.; Ming-Wei, Kang; Huan-Cheng, Chang; Kuan-Ming, Chen.; Yu., Y.-C. Bright Fluorescent Nanodiamonds: No Photobleaching and Low Cytotoxicity. *J. Am. Chem. Soc.* **2005**, *127*, 17604–17605.
4. Faklaris, O.; Garrot, D.; Joshi, V.; Druon, F.; Boudou, J. P.; Sauvage, T.; Georges, P.; Curmi, P. A.; Treussart, F. Detection of Single Photoluminescent Diamond Nanoparticles in Cells and Study of the Internalization Pathway. *Small* **2008**, *4*, 2236–2239.
5. Chi-Cheng, Fu.; Hsu-Yang, Lee.; Kowa, Chen.; Tsong-Shin, Lim.; Hsiao-Yun, Wu.; Po-Keng, Lin.; Pei-Kuen, Wei.; Pei-Hsi, Tsao.; Huan-Cheng, Chang.; Fann, W. Characterization and Application of Single Fluorescent Nanodiamonds as Cellular Biomarkers. *Proc. Natl. Acad. Sci. U.S.A.* **2007**, *104*, 727–732.
6. Wee, T.-L.; Mau, Y.-W.; Fang, C.-Y.; Hsu, H.-L.; Han, C.-C.; Chang, H.-C. Preparation and Characterization of Green Fluorescent Nanodiamonds for Biological Applications. *Diamond Relat. Mater.* **2009**, *18*, 567–573.
7. Liu, K.-K.; Cheng, C.-L.; Chang, C.-C.; Chao, J.-I. Biocompatible and Detectable Carboxylated Nanodiamond on Human Cell. *Nanotechnology* **2007**, *18*, 325102/1–325102/10.
8. Chang, I. P.; Hwang, K. C.; Chiang, C.-S. Preparation of Fluorescent Magnetic Nanodiamonds and Cellular Imaging. *J. Am. Chem. Soc.* **2008**, *130*, 15476–15481.
9. Liu, K.-K.; Chen, M.-F.; Chen, P.-Y.; Lee, T. J. F.; Cheng, C.-L.; Chang, C.-C.; Ho, Y.-P.; Chao, J.-I. Alpha-Bungarotoxin Binding to Target Cell in a Developing Visual System by Carboxylated Nanodiamond. *Nanotechnology* **2008**, *19*, 205102/1–205102/10.
10. Vial, S.; Mansuy, C.; Sagan, S.; Irinopoulou, T.; Burlina, F.; Boudou, J.-P.; Chassaing, G.; Lavielle, S. Peptide-Grafted Nanodiamonds: Preparation, Cytotoxicity, and Uptake in Cells. *ChemBioChem* **2008**, *9*, 2113–2119.
11. Zhang, X.-Q.; Chen, M.; Lam, R.; Xu, X.; Osawa, E.; Ho, D. Polymer-Functionalized Nanodiamond Platforms as Vehicles for Gene Delivery. *ACS Nano* **2009**, *3*, 2609–2616.
12. Shimkunas, R. A.; Robinson, E.; Lam, R.; Lu, S.; Xu, X.; Zhang, X.-Q.; Huang, H.; Osawa, E.; Ho, D. Nanodiamond-Insulin Complexes as PH-Dependent Protein Delivery Vehicles. *Biomaterials* **2009**, *30*, 5720–5728.
13. Chen, M.; Pierstorff, E. D.; Lam, R.; Li, S.-Y.; Huang, H.; Osawa, E.; Ho, D. Nanodiamond-Mediated Delivery of Water-Insoluble Therapeutics. *ACS Nano* **2009**, *3*, 2016–2022.
14. Aihui, Yan.; Bonnie, W. Lau.; Bevan, S. Weissman.; Indrek, Külaots.; Nancy, Y. C. Yang.; Agnes, B. Kane.; Hurt, R. H. Biocompatible, Hydrophilic, Supramolecular Carbon Nanoparticles for Cell Delivery. *Adv. Mater.* **2006**, *18*, 2373–2378.
15. Shenderova, O. A.; Zhirnov., V. V.; Brenner, D. W. Carbon Nanostructures. *Crit. Rev. Solid State Mater. Sci.* **2002**, *27*, 227.
16. Krueger, A. Diamond Nanoparticles: Jewels for Chemistry and Physics. *Adv. Mater.* **2008**, *20*, 2445–2449.
17. Zhu, Z. B. Detonation of Molecular Precursors as a Tool for the Assembly of Nano-Sized Materials. *Mod. Phys. Lett.* **2003**, *17*, 1477–1493.
18. Ya-Ping, S.; Bing, Z.; Yi, L.; Wei, W.; K. A.; Shiral, F.; Pankaj, P.; Jaouad Meziani, M.; Harruff, B.A. ; Wang, X.; Wang, H. Quantum-Sized Carbon Dots for Bright and Colorful Photoluminescence. *J. Am. Chem. Soc.* **2006**, *128*, 7756–7757.
19. Martin, R.; Heydorn, P. C.; Alvaro, M.; Garcia, H. General Strategy for High-Density Covalent Functionalization of Diamond Nanoparticles Using Fenton Chemistry. *Chem. Mater.* **2009**, *21*, 4505–4514.

20. Sokolova, V.; M., E. Inorganic Nanoparticles as Carriers of Nucleic Acids into Cells. *Angew. Chem., Int. Ed.* **2008**, *47*, 1382–1395.
21. Mochalin, N.; Gogotsi, Y. Wet Chemistry Route to Hydrophobic Blue Fluorescent Nanodiamond. *J. Am. Chem. Soc.* **2009**, *131*, 4594–4595.
22. Spitsyn, B. V.; Gradoboev, M. N.; Galushko, T. B.; Karpukhina, T. A.; Serebryakova, N. V.; Kulakova, I. I.; Melnik, N. N. Purification and Functionalization of Nanodiamond. *NATO Sci. Ser. II* **2005**, *192*, 241–252.
23. Antonov, L.; Gergov, G.; Petrov, V.; Kubista, M.; Nygren, J. UV−Vis Spectroscopic and Chemometric Study on the Aggregation of Ionic Dyes in Water. *Talanta* **1999**, *49*, 99–106.
24. Khairutdinov, R. F.; Serpone, N. Photophysics of Cyanine Dyes: Subnanosecond Relaxation Dynamics in Monomers, Dimers, and H- and J-Aggregates in Solution. *J. Phys. Chem. B* **1997**, *101*, 2602–2610.
25. Gemeay, A. H.; Mansour, I. A.; El-Sharkawy, R. G.; Zaki, A. B. Kinetics of the Oxidative Degradation of Thionine Dye by Hydrogen Peroxide Catalyzed by Supported Transition Metal Ions Complexes. *J. Chem. Technol. Biotechnol.* **2004**, *79*, 85–96.
26. Li, W.; Zhang, N.; Liang, X.; Li, J.; Gong, P.; Yu, X.; Ma, G.; Ryan, U. M.; Zhang, X. Transient Transfection of Cryptosporidium Parvum Using Green Fluorescent Protein (GFP) as a Marker. *Mol. Biochem. Parasitol.* **2009**, *168*, 143–148.
27. Ramirez, S. M.; Moon, N. G.; Lang, M. A.; Layman, J. M.; Long, T. E. Synthesis of Functional Ionenes for Nonviral Gene Transfection. *Polym. Prepr. (Am. Chem. Soc., Div. Polym. Chem.)* **2009**, *50*. No pp given.
28. Lynn, D. M.; Anderson, D. G.; Putnam, D.; Langer, R. Accelerated Discovery of Synthetic Transfection Vectors: Parallel Synthesis and Screening of a Degradable Polymer Library. *J. Am. Chem. Soc.* **2001**, *123*, 8155–8156.
29. Qian, Y. F.; Gu, M. C. Cationic Liposomes in Gene Transfection Vectors. *Zhongguo Yaoshi (Wuhan, China)*. **2008**, *11*, 1041–1043.
30. Ewert, K. K.; Samuel, C. E.; Safinya, C. R. Lipid-DNA Interactions: Structure−Function Studies of Nanomaterials for Gene Delivery. *DNA Interact. Polym. Surfactants* **2008**, 377–404.
31. Maee, M.; El Andaloussi, S.; Lundin, P.; Oskolkov, N.; Johansson, H. J.; Guterstam, P.; Langel, U. A Stearylated CPP for Delivery of Splice Correcting Oligonucleotides Using a Noncovalent Co-incubation Strategy. *J. Controlled Release* **2009**, *134*, 221–227.